Resolving natural organic matter and nanoplastics in binary or ternary systems via UV–Vis analysis

Journal of Colloid and Interface Science

Zhang, Ran; Chen, Yali; Ouyang, Xiaoxue; Weng, Liping; Ma, Jie et al

https://doi.org/10.1016/j.jcis.2022.11.050

Journal of Colloid and Interface Science 632 (2023) 335–344

Contents lists available at ScienceDirect

Journal of Colloid and Interface Science

journal homepage: www.elsevier.com/locate/jcis

Resolving natural organic matter and nanoplastics in binary or ternary systems via UV–Vis analysis

Ran Zhang [a], Yali Chen [a,*], Xiaoxue Ouyang [a], Liping Weng [a,b,*], Jie Ma [a], Md. Shafiqul Islam [c], Yongtao Li [d]

[a] Agro-Environmental Protection Institute, Ministry of Agriculture and Rural Affairs / Key Laboratory of Original Agro-Environmental Pollution Prevention and Control, MARA / Tianjin Key Laboratory of Agro-Environment and Agro-Product Safety, Tianjin 300191, China
[b] Department of Soil Quality, Wageningen University, P.O. Box 47, 6700 AA, Wageningen, the Netherlands
[c] Department of Civil and Environmental Engineering, Shantou University, Shantou 515063, China
[d] College of Natural Resources and Environment, South China Agricultural University, Guangzhou 510642, China

HIGHLIGHTS

- The UV–Vis method can identify the fingerprints of PSNPs and NOM in their mixtures.
- Preferential adsorption of NOM to goethite decreased NOM's specific absorbance.
- The method performs well for PSNPs-original NOM system with detection limits of 7.4 and 20.8 mgC L^{-1}, respectively.
- The method performs well for PSNPs-fractionated NOM system with detection limits of 27.5 and 31.2 mgC L^{-1}, respectively.
- The UV–Vis method can quantify the NOM proportion that interacts with the PSNPs.

GRAPHICAL ABSTRACT

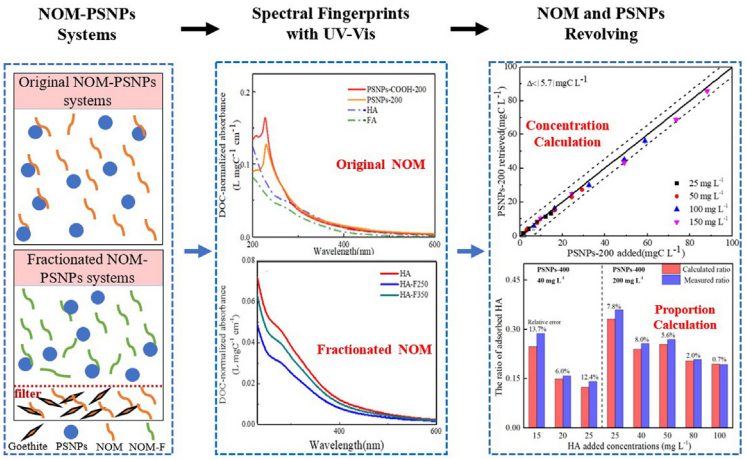

ARTICLE INFO

Article history:
Received 31 March 2022
Revised 18 October 2022
Accepted 10 November 2022
Available online 15 November 2022

Keywords:
Nanoplastics
Natural organic matter
Adsorptive fractionation
UV–Vis spectroscopy

ABSTRACT

Nanoplastics (NPs) and natural organic matter (NOM) are ubiquitous and usually present simultaneously in the environment. Both NPs and NOM can be adsorbed to minerals such as iron-(hydr)oxides, with such interactions being important for controlling their fate in the environment. However, the quantification of NPs and NOM in mixtures remains challenging even under controlled conditions in laboratory studies. In this research, a UV–Vis method was established to quantify concentrations of NOM, such as humic acid (HA) and fulvic acid (FA), and polystyrene NPs (PSNPs) in mixtures. In addition, both original NOM samples and those recovered following adsorptive fractionation using an iron oxide (goethite, α-FeOOH) were mixed separately with PSNPs and their concentrations were further calculated via the developed UV–Vis method. The UV–Vis method performed well (recovery of 100 ± 16 %) with original NOM and PSNPs system at detection limits of 20.8 and 7.4 mgC L^{-1}, respectively. Particularly, for original FA and PSNPs systems with carboxylic groups (PSNPs-COOH, 200 nm), a similar recovery rate could be obtained at detection limits of only 2.5 and 1.9 mgC L^{-1}, respectively. For fractionated NOM and PSNPs systems, detection limits (31.2 mgC L^{-1} and 27.5 mgC L^{-1}, respectively) are increased to reach the same accuracy. Furthermore, the UV–Vis method can be used to estimate the proportion of HA that is adsorbed to PSNPs. The relative errors are < 13.7 % when the mass ratios of PSNPs and HA was between 1.6:1 and 8:1 and HA

* Corresponding authors at: Agro-Environmental Protection Institute, Ministry of Agriculture and Rural Affairs, Tianjin 300191, China.
E-mail addresses: chenyali@caas.cn, liping.weng@wur.nl (L. Weng).

https://doi.org/10.1016/j.jcis.2022.11.050

concentration was higher than 4.6 mgC L^{-1}. This method developed can be applied to future laboratory research to investigate the interaction between NOM, NPs, and minerals.

1. Introduction

Millions of tons of plastic are produced and used in industry, agriculture, and daily life each year [1]; consequently, plastic pollution in the environment has become a serious health and safety concern. Large plastic debris can break down into microplastics (MPs, 1–5 mm) and nanoplastics (NPs, 1–1000 nm) through fragmentation processes under ultraviolet radiation (UV), biodegradation, and weathering [2–6]. As an emerging contaminant, NPs have recently received considerable attention and are widely detected in the air, sea, sludge, surface water and soil [7–11]. Compared to the aquatic environment, there are more NPs in terrestrial environment [12]. NPs contain hazardous substances, such as bisphenol A, phthalates, poly brominated diphenyl ethers, and heavy metals used in coloring [13–15]. Additionally, owing to their large specific surface area, surface charges, functional groups, and hydrophobicity, NPs can adsorb contaminants, such as heavy metals and persistent organic pollutants, and then co-migrate, further increasing their environmental risk [16–19]. NPs can also be taken up by plants and ingested by animals (such as the Japanese medaka *Oryzias latipes*), ultimately altering gene expression, causing stress effects on the liver, and damaging the respiratory, digestive, and circulatory systems of affected animals [20–22]. Therefore, it is of great significance to study the environmental behavior of NPs in the terrestrial system. The environmental behavior of NPs in soil is mainly controlled by soil components, among which natural organic matter (NOM) and minerals (such as iron-(hydr)oxides) are the most important factors.

NOM, which is mainly derived from the residues of plants, microorganisms, and animals, is widely present in soil. NOM includes humic substances, which are classified as humic acid (HA), fulvic acid (FA), and humin according to their solubility in acidic and basic solutions [23]. Notably, previous studies have indicated that NOM can interact with plastics [24,25]. For instance, Shiu et al. [26] reported that dissolved organic matter (DOC) tended to form particulate organic matter via its hydrophobic interactions with NPs. Chen et al. [25] found that polystyrene NPs (PSNPs) interacted with the aromatic structure of HA via π–π conjugation, being surrounded by the carboxyl and C═O bonds in HA to form a highly conjugated co-polymer. These interactions could affect the physical and chemical behaviors of both NOM and plastics. For example, the presence of HA significantly inhibited the aggregation of polyethylene glycol terephthalate NPs [27].

As a ubiquitous mineral with strong surface reactivity in soil, iron-(hydr)oxides can act as an adsorbent for both NPs and NOM [28,29]. It has been shown that the adsorption of PSNPs onto the surface of iron oxide varied with the type of iron oxide [29], and the adsorption of PSNPs on goethite was stronger than on magnetite [30]. The adsorption of NOM on iron-(hydr)oxides has also been studied extensively and shown to involve adsorption mechanisms such as electrostatic interaction, ligand exchange, cation bridging, H-bonding, hydrophobic interaction, and van der Waals interaction [28,31–37]. Moreover, preferential adsorption of certain fractions of NOM to iron oxides can occur owing to the chemical heterogeneity and polydispersity of NOM [33,38–41]. Several studies showed that the fraction of NOM with lower molar mass exhibited greater affinity for goethite and hematite [33,42], while another study indicated that larger molecules of FA and intermediate sized molecules of HA were preferentially adsorbed to goethite [41].

In studying NPs adsorption to iron oxide, the amount of adsorbed NPs can easily be quantified by measuring NPs concentration remaining in the supernatant after centrifugation; the same approach holds for measuring adsorption of NOM to iron oxide. However, in a solution consisting of both NPs and NOM, it is technically difficult to distinguish between the two components because they are both in nanometer sizes and have similar mass densities. Thus, many previous laboratory-based studies focused on the characterization of NPs and NOM without quantification, whereas others used plastics of larger sizes (e.g. 10 μm) that could be filtered out to quantify NOM remaining in the filtrate [43]. To date, little laboratory-based research has been performed with regard to multicomponent systems that include NPs, NOM, and minerals, in part because of the lack of analytical methods that can effectively quantify NPs and NOM in a fractioned equilibrium solution. Moreover, in the soil, HA and FA usually coexist, and preferential adsorption of certain fractions of HA and FA to iron oxide have been observed [41]. Thus, the presence of fractionated NOM through preferential adsorption renders the determination of NOM and NP concentrations in a mixture even more challenging.

UV–visible light spectroscopy (UV–Vis) is a conventional and convenient analytical method that is based on the principle that different substances have distinct light absorption spectra and intensities caused by the transitions of electrons within their molecular structures. Using the UV–Vis method, the concentrations of PSNPs have been measured at wavelengths of 225, 227.5, and 250 nm [44–46], whereas those of NOM (i.e., HA and FA) were measured at 254, 365, and 465 nm [38,47,48]. A previous study also determined the PSNPs concentration at a wavelength of 227.5 nm in the presence of NOM, in which the light absorption of NOM was ignored [45]. However, the UV–Vis wavelength range over which both NPs and NOM have light absorption overlaps; therefore, use of a specific wavelength to determine the concentration either NPs or NOM does not yield accurate results when the substances are mixed together. Recently, an UV–Vis method for quantifying HA and FA that have similar absorbance wavelength range has been established, which used the characteristics of the whole spectra over a wavelength of 230–600 nm instead of a single wavelength and the relative error of this method is within 25 % when the concentrations of HA and FA are higher than 18 mgC L^{-1} [49].

In this study, we aimed to establish a fast and convenient UV–Vis method that can not only quantify the concentrations of both NPs and NOM in a mixture but also determine the proportion of NOM that interacts with the NPs. Moreover, as the properties of NOM may change because of their preferential adsorption to minerals such as iron oxides, an additional challenge is to consider the influence of this preferential adsorption on the analysis. In this research, PSNPs with a diameter of 200 and 400 nm (PSNPs-200 and PSNPs-400) and PSNPs modified with –COOH group with a diameter of 200 nm (PSNPs–COOH-200) were used as model NPs, as these have been used extensively in previous laboratory-based studies [25,30,50]. HA and FA were chosen as representative NOM while goethite as a representative iron oxide. Mixtures involving PSNPs along with original and fractionated HA (HA-F) or FA (FA-F) were used to establish and assess the UV–Vis methodology. To evaluate the feasibility, accuracy, and limitations of this

method, the measured concentrations were compared to known added values. This developed analytical method is expected to advance future laboratory-based studies of ternary systems including NPs, NOM, and iron oxide, which will contribute to further clarification of the environmental behavior of NPs.

2. Material and methods

2.1. Primary materials

HA and FA were extracted from the A soil horizon collected from a forest in Jilin Province, China (42°10′10.49″ N, 124°37′25.24″ E) following the protocols of the International Humic Substances Society (IHSS). A detailed description of this procedure can be found elsewhere [51,52]. The purified HA and FA were freeze-dried and stored at 4 °C in the dark. The weight average molar mass (M_W) of the HA and FA, measured using size exclusion chromatography was 15.4 and 2.0 kDa, respectively; the fourier transform infrared spectra (Nicolet iS20, Thermo Scientific, Waltham, MA, USA) are shown in Fig. S1c. PSNPs (PSNPs-200, PSNPs–COOH-200, and PSNPs-400) were obtained from Welab Biotechnology Co. (Beijing, China) at a concentration of 5 % (w/v).

The carbon contents of HA, FA, PSNPs-200, PSNPs–COOH-200 and PSNPs-400 were 46.3, 40.0, 65.3, 73.2, and 65.0 %, respectively, as determined by measuring the total organic carbon (TOC) contents (MultiN/C 3100, Analytik Jena, Germany) in solutions of known HA, FA, and PSNP concentrations. The HA stock solution (1 g L^{-1}) was prepared by dissolving freeze-dried HA in NaOH solution at pH = 11, and that of FA (0.5 g L^{-1}) was prepared by dissolving the freeze-dried FA material in ultrapure water. Then, both stock solutions were equilibrated for 24 h and filtered through a 0.45-μm polyether sulfone filter. All the stock solutions of PSNPs (1 g L^{-1}) were prepared by diluting the original suspension (5 %) with ultrapure water.

2.2. Fractionation of HA and FA

To evaluate the effect of adsorptive fractionation on the quantification of HA and FA, goethite suspensions with HA or FA were prepared from the original stocks. Goethite was prepared according to the procedures described in Hiemstra and Van Riemsdijk [53]. The specific surface area of this goethite as measured using Brunauer-Emmett-Teller adsorption isotherms, is 87.65 m^2 g^{-1} and the pristine point of zero charge is pH = 9.3, as described in our previous study [54]. The initial concentrations for HA were 250, 300, 350, and 400 mg L^{-1} with 3.0 g L^{-1} goethite, designated as HA-F250, HA-F300, HA-F350, and HA-F400, respectively. The initial concentrations for FA were 100, 150, 200, and 250 mg L^{-1} with 3.0 g L^{-1} goethite, designated as FA-F100, FA-F150, FA-F200, and FA-F250, respectively. For all mixtures, the ionic strength was adjusted to 0.001 mol L^{-1} using NaCl, and the pH was adjusted to 6.0 using 0.01 mol L^{-1} HCl and 0.01 mol L^{-1} NaOH. After shaking for two days at 20 ± 1 °C in the dark, the suspensions were centrifuged (10000 rpm, 30 min), then the supernatant was filtered through a 0.45-μm filter and filtrate was considered as the fractionated NOM. Then, the TOC content in the filtrate was measured using a TOC analyzer, with the value regarded as the concentration of fractionated NOM. The results showed that the percentage of HA and FA adsorbed to goethite were 21.8–52.0 % and 33.2–90.3 % respectively (Table S1).

2.3. Preparation of test solutions

In total, three series of test solutions of PSNPs, original HA and FA as well as HA-F and FA-F were prepared (Table S2). In the first two series, mixtures of PSNPs were prepared with either original (first series) or fractionated (second series) HA or FA at different HA or FA to PSNPs ratios. These solutions were used to develop the UV–Vis method. In the third series, mixtures of PSNPs were prepared with varying concentrations of HA to evaluate the interaction of NOM with PSNPs. All test solutions were carried out in triplicate and solutions containing only PSNPs, HA, or FA were also prepared and used as controls. According to the results of transmission electron microscopy (TEM, FEI Tecnai F20) and time-resolved dynamic light scattering (DLS, Zetasizer Nano ZS, Malvern Instruments; Figs. S2 and S3), the addition of NOM in this study did not induce the aggregation of PSNPs.

2.3.1. Series 1: Mixtures of original NOM with PSNPs at different total concentrations and ratios

The original HA or FA were mixed with PSNPs (PSNPs-200, PSNPs–COOH-200, and PSNPs-400) at total mass (HA or FA + PSNPs) concentrations of 25, 50, 100, or 150 mg L^{-1}, and mass ratios of HA or FA to PSNPs at 1:9, 1:3, 1:1, 3:1, and 9:1. To better determine the accuracy of the UV–Vis method, a wide range of NPs and NOM concentrations (2.5–135 mg L^{-1}) were adopted, as reported in previous laboratory-based studies [25,41,50,55]. Additionally, a ternary system containing HA, FA, and PSNPs (PSNPs–COOH-200) was prepared at total concentrations of 100 and 150 mg L^{-1}. The mass ratios of the total NOM (HA + FA) to PSNPs were also 1:9, 1:3, 1:1, 3:1, or 9:1; the mass ratio of HA to FA was kept constant at 1.5:1.

2.3.2. Series 2: Mixtures of fractionated NOM and PSNPs at different total concentrations and ratios

HA-F and FA-F were prepared based on the percentage of HA or FA adsorbed to goethite as determined by TOC assessment (Section 2.2; Table S1). HA-F (HA-F250 and HA-F350) was prepared from the filtrate of the 250 and 350 mg L^{-1} HA with 3.0 g L^{-1} goethite, and FA-F (FA-F200 and FA-F250) was prepared from the filtrate of the 200 and 250 mg L^{-1} FA with 3.0 g L^{-1} goethite. PSNPs–COOH-200 and PSNPs-200 were mixed with HA-F at a total concentration of 100 mg L^{-1} and with FA-F at a total concentration of 80 mg L^{-1}. The mixtures of HA-F or FA-F and PSNPs were prepared at mass ratios of HA-F or FA-F:PSNPs = 1:9, 1:3, 1:1, 3:1, and 9:1. Furthermore, a ternary system was prepared containing HA-F350, FA-F250, and PSNPs–COOH-200 at a total concentrations of 150 mg L^{-1}. The mass ratios of the total fractioned NOM (HA-F350 + FA-F250) to PSNPs–COOH-200 in this system were 1:9, 1:3, 1:1, 3:1, or 9:1, and the mass ratio of HA-F350 to FA-F250 was kept constant at 1.5:1.

2.3.3. Series 3: Mixtures of original HA with PSNPs at different HA concentrations

To further calculate the proportion of NOM that interacts with the PSNPs, HA was selected as a representative NOM and different concentrations (2.5, 5, 10, 15, 20, 25, 30, 40, 50, 80, and 100 mg L^{-1}) were mixed with 40 mg L^{-1} PSNPs-400. Additionally, another binary adsorption experiment was conducted with elevated concentrations of PSNPs-400 (200 mg/L) and HA (12.5, 25, 40, 50, 80, and 100 mg L^{-1}) to increase the proportion of HA interacted with PSNPs. After reaching equilibrium, the mixtures were centrifuged (10000 rpm, 30 min) and the supernatant was filtered through a 0.22-μm filter to remove the PSNPs-400; unabsorbed HA in the filtrate was directly measured using a TOC analyzer.

For all mixtures, the ionic strength was maintained at 0.001 mol L^{-1} using NaCl and the pH was adjusted to 6.0. Based on the preliminary kinetic experiments (Fig. S4), the samples were equilibrated on a shaker at 20 ± 1 °C in the dark for seven days before quantifying the concentrations of PSNPs, HA, or FA. TOC content

was measured using a TOC analyzer and UV–Vis light absorbance was measured as described in section 2.4.

2.4. UV–Vis spectroscopy

To avoid the influence of pH on the UV–Vis spectroscopic measurements, 0.01 mol L^{-1} phosphate buffer was used to adjust the pH to 6.9 for each sample prior to the measurements. In addition, samples with absorbance of > 1 unit were diluted to ensure the accuracy of the UV–Vis measurement. The UV–Vis spectra of the samples were collected using a spectrophotometer (UV-2700, Shimadzu, Kyoto, Japan) over the wavelength range of 200–600 nm with a resolution of 1 nm. The relative error of instrument was <3 % (Table S3). The detectable concentrations of HA and NPs were determined by spectrophotometer (Fig. S5), and HA and NPs concentrations at 1 mg L^{-1} could also be detected, which met our experimental requirements (the minimum experimental concentration is 2.5 mg L^{-1}). The first order derivatives of the spectra were acquired and smoothed using an interval of 17 data points using Origin 8.5 software [56]. The PSNPs and NOM concentrations in the mixtures were then derived using a fitting method established as described in results and discussion.

3. Results and discussion

3.1. Mixtures of original NOM and PSNPs

3.1.1. UV–Vis spectra of the original NOM and PSNPs

The DOC-normalized UV–Vis spectra of the original NOM and PSNPs differed significantly (Fig. 1a). The PSNPs (PSNPs–COOH-200 and PSNPs-200) exhibited one distinct peak in the spectra around 228 nm, whereas NOM showed no evident peaks. The carbon-normalized specific absorbance of PSNPs–COOH-200 was higher than that of PSNPs-200 in the wavelength range of 200–260 nm, whereas the specific absorbance of HA was higher than that of FA over the entire wavelength range. The spectral difference between PSNPs–COOH-200 and NOM was greater than that between PSNPs-200 and NOM. Moreover, the trend of specific absorbance decrement was slightly faster for PSNPs than for NOM over 228–300 nm. However, the first order derivatives of the DOC-normalized spectra (Fig. 1b) revealed only slight differences between the NOM and PSNPs at wavelengths > 300 nm, which illustrated there was little difference in the shape of the spectra between the NOM and PSNPs at a wavelength > 300 nm.

3.1.2. UV–Vis method development

If no interaction exists between NOM and PSNPs, the spectrum of the mixture can be considered as a simple sum of the spectra of NOM and PSNPs based on Eq. (1a), and the concentrations of NOM and PSNPs in mgC L^{-1} in an unknown mixture can be obtained using Eq. (1b).

$$TS_{MIX(i)} = \alpha R_{NOM(i)} + (1-\alpha) R_{PSNPs(i)} \quad (1a)$$

where $R_{NOM(i)}$ (L mgC^{-1} cm^{-1}) and $R_{PSNPs(i)}$ (L mgC^{-1} cm^{-1}) represent the specific absorbance of NOM or PSNPs in the reference spectra at a certain wavelength of i nm. The reference spectra were obtained by measuring NOM or PSNPs samples with a known concentration. $TS_{MIX(i)}$ (L mgC^{-1} cm^{-1}) represents the specific absorbance of the mixture sample at the same wavelength (i nm); α is the NOM carbon mass fraction in the mixture and 1 – α is the PSNPs carbon mass fraction in the mixture.

$$\begin{aligned} C_{NOM} &= \alpha \times TOC_{mix} \\ C_{PSNPs} &= (1-\alpha) \times TOC_{mix} \end{aligned} \quad (1b)$$

where $C_{NOM\ (mgC\ L^{-1})}$ and C_{PSNPs} (mgC L^{-1}) are concentrations of NOM and PSNPs, respectively, and TOC_{mix} (mgC L^{-1}) is the TOC concentration measured in the mixture.

However, interactions did occur between HA and PSNPs, likely through hydrophobic interaction and π–π bonds [24,25]. Thus, to reflect the influence of the interaction between the NOM and PSNPs on the UV–Vis light absorbance, two additional parameters, β and γ, were introduced compared to Eq. (1a) as shown in Eq. (2a).

$$TS_{MIX(i)} = \alpha\beta R_{NOM(i)} + (1-\alpha)\gamma R_{PSNPs(i)} \quad (2a)$$

where β and γ are used to describe the change of specific absorbance for NOM and PSNPs caused by interactions between them, expressed by Eq. S4. Therefore Eq. (2a) can be rewritten as follows:

$$TS_{MIX(i)} = AR_{NOM(i)} + BR_{PSNPs(i)} \quad (2b)$$

where $A = \alpha\beta$ and $B = (1-\alpha)\gamma$, assuming β and γ are constants for any wavelength; i.e., the interaction between NOM and PSNPs changes the intensity of the spectra with the same proportion, but the interaction does not change the shape of the spectra (Fig. S6). A and B can be obtained by fitting the equation to the spectra of the mixture of NOM and PSNPs, minimizing the sum of squared differences between the measured and calculated total absorbance $\left(\Sigma\left(TS_{MIX(i)} - TS_{MIX(i)(model)}\right)^2\right)$ over the selected range of wavelength. The NOM fraction ($\alpha = A/(A+B)$) in the mixture can be acquired using the fitted values of A and B. Then, the concentrations of NOM and PSNPs can be calculated by combining α and the TOC analysis of the mixture (TOC_{mix}) as described in Eq. (1b).

The method was tested in systems with original NOM and PSNPs, using the entire wavelength range (200–600 nm) and two sub-ranges (200–230 and 231–600 nm). These sub-ranges were chosen because although the specific absorbance of NOM and

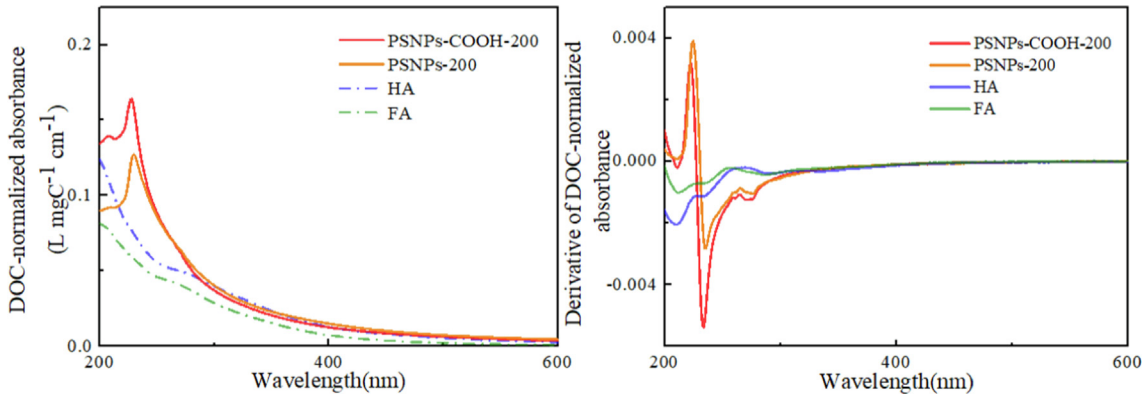

Fig. 1. Carbon normalized UV–Vis spectra and derivatives of the DOC-normalized UV–Vis spectra of the original HA, FA, and PSNPs.

PSNPs differed most over 200–230 nm (Fig. 1), the stability and replicability of the absorbance for the mixture are higher in the range of 231–600 nm (Fig. S7). The instability of the spectra over 200–231 nm can be caused by interference of air and water moisture. This interference is well known for far ultraviolet wavelengths (<200 nm). Taking the mixture of HA and PSNPs-200 as an example, better recoveries (calculated as the ratio of the estimated concentration to the known added concentration) were obtained using the 231–600 nm wavelength range than those from 200 to 230 and 200–600 nm at different total (HA + PSNPs-200) concentrations (Table 1). The HA recovery using spectra over 231–600 nm was 98.1–248.6 %, whereas the error became larger using spectra over 200–230 nm (recovery of −72.1–729.5 %) and 200–600 nm (recovery of 52.3–604.4 %) wavelength ranges. Similarly, the best recoveries (88.3–112.0 %) were obtained for PSNPs-200 using spectra over 231–600 nm (Table 1). Thus, the wavelength range over 231–600 nm was used to derive the concentrations of the original HA and PSNPs-200, yielding 100 ± 16 % recovery for HA and PSNPs-200 with detection limits of 20.8 and 1.7 mgC L^{-1}, respectively (Fig. 2). Additionally, HA recovery within 100 ± 16 % was also obtained when the mass fraction of HA in the mixture was > 0.25, even though the HA concentration in the mixture was < 20.8 mgC L^{-1}. For example, HA recovery improved from 248.6 % and 135.7 % at a mass fraction of 0.1 and 0.25, respectively, to 100.3, 98.8, and 98.1 % at a mass fraction of 0.5, 0.75, and 0.9 and a total concentration of 25 mg L^{-1} (with HA concentrations of 5.8, 8.7, and 10.4 mgC L^{-1}, respectively (Table 1). This may be because only a small proportion of HA reacts with PSNPs when the mass fraction of HA is higher, and the effect caused by such interaction on the UV–Vis method is smaller.

The wavelength region over 231–600 nm was also more suitable for measuring concentrations in the FA and PSNPs systems with relatively higher recoveries obtained for FA and PSNPs than those using spectra over wavelength ranges of 200–300 and 200–600 nm (Table S4). In the FA and PSNPs-200 system, the recovery was 100 ± 16 % with FA and PSNPs-200 detection limits of 7.5 and 4.1 mgC L^{-1}, respectively (Fig. S8a). Thus, compared to the HA and PSNPs system, similar relative errors were obtained for FA and PSNPs mixtures even at a relatively lower detection limit. The better performance of the method for FA than for HA might result from: 1) compared to HA, FA has more hydrophilic groups (such as hydroxyl or carboxyl) and higher charge density (Fig. S1c), resulting in weaker hydrophobicity and fewer interactions with PSNPs; 2) the difference between FA and PSNPs of the DOC-normalized UV–Vis spectra over 231–600 nm is larger than that between HA and PSNPs (Fig. 1), which leads to easier discrimination of FA and PSNPs.

3.1.3. Effects of a carboxylic functional group on PSNPs

For the mixtures of HA with PSNPs–COOH-200, better measurements were obtained using spectra over the 231–600 nm wavelength range than those over 200–230 and 200–600 nm (Table S5). The HA and PSNPs–COOH-200 recoveries derived using the spectra over 231–600 nm were 56.0–100.5 % and 97.3–161.8 %, respectively, across the total concentrations and HA to PSNPs proportions evaluated. The estimated concentrations of the original HA and PSNPs-COOH-200 were consistent with the added contents (within 100 ± 16 % recovery) for HA detection limit of 8.7 mgC L^{-1} and PSNPs–COOH-200 detection limit of 3.7 mgC L^{-1} (Fig. S8c). Notably, as shown in Fig. 2, to achieve the same recovery (100 ± 16 %), a lower HA detection limit (8.7 mgC L^{-1}) was required than in the presence of PSNPs-200 (20.8 mgC L^{-1}). The higher accuracy obtained in the system with PSNPs–COOH-200 (Δ < ±2.9 mgC L^{-1}, Fig. S8c) compared to that with PSNPs-200 (Δ < ±5.7 mgC L^{-1}, Fig. 2) might result from the relatively weaker hydrophobicity of PSNPs–COOH-200 (Figs. S1a and S1b), leading to a lesser interaction with HA [26].

In the mixtures with FA, a similar effect of the carboxylic functional group of PSNPs on the measurement was observed (Table S4). The UV–Vis method also performed better in the system

Table 1
Recoveries (%) for HA and PSNPs-200 derived from Eq. (1b) and (2b) using the UV–Vis spectra over 200–600 nm, 200–230 nm and 231–600 nm for mixture samples containing the original HA and PSNPs-200.

	HA mass fraction	HA recoveries %			PSNPs-200 recoveries %		
		200–600 nm	200–230 nm	231–600 nm	200–600 nm	200–230 nm	231–600 nm
HA+	0.1	604.4	729.5	248.6	60.3	50.5	88.3
PSNPs-200	0.25	164.5	139.4	135.7	84.8	81.3	91.6
25 mg/L	0.5	158.3	158.7	100.3	58.7	58.5	99.8
	0.75	148.9	124.6	98.8	46.3	47.8	102.7
	0.9	112.9	97.5	98.1	53.5	116.2	112.0
	Average	237.8	249.9	136.3	60.7	70.9	98.8
	s.d.	184.2	240.7	57.9	13.0	25.5	8.4
HA+	0.1	231.8	230.4	199.5	89.6	89.8	92.2
PSNPs-200	0.25	209.5	229.7	127.9	74.2	69.4	93.4
50 mg/L	0.5	131.5	124.1	111.7	77.7	82.9	91.7
	0.75	121.9	109.9	103.1	53.6	78.9	93.4
	0.9	105.5	94.1	99.0	65.2	137.8	106.7
	Average	160.0	157.6	128.2	72.0	91.8	95.5
	s.d.	50.7	59.9	37.0	12.1	24.0	5.7
HA+	0.1	77.0	96.1	158.5	101.8	107.9	95.4
PSNPs-200	0.25	132.8	137.1	133.6	92.3	91.2	92.1
100 mg/L	0.5	128.9	136.5	111.6	79.6	74.2	91.8
	0.75	66.7	71.2	100.6	170.9	161.3	98.7
	0.9	82.9	90.4	102.4	209.1	161.4	103.7
	Average	97.6	106.2	121.4	130.7	119.2	96.3
	s.d.	27.6	26.3	22.0	50.4	36.0	4.5
HA+	0.1	52.3	−72.1	133.3	103.8	113.6	97.4
PSNPs-200	0.25	161.6	191.4	126.6	85.5	78.4	93.7
150 mg/L	0.5	75.0	75.0	116.3	117.7	117.7	88.4
	0.75	119.2	111.0	99.2	59.2	76.6	101.8
	0.9	77.0	84.6	99.4	246.7	198.0	104.2
	Average	97.0	78.0	115.0	122.6	116.8	97.1
	s.d.	38.8	85.5	13.9	65.1	44.0	5.6

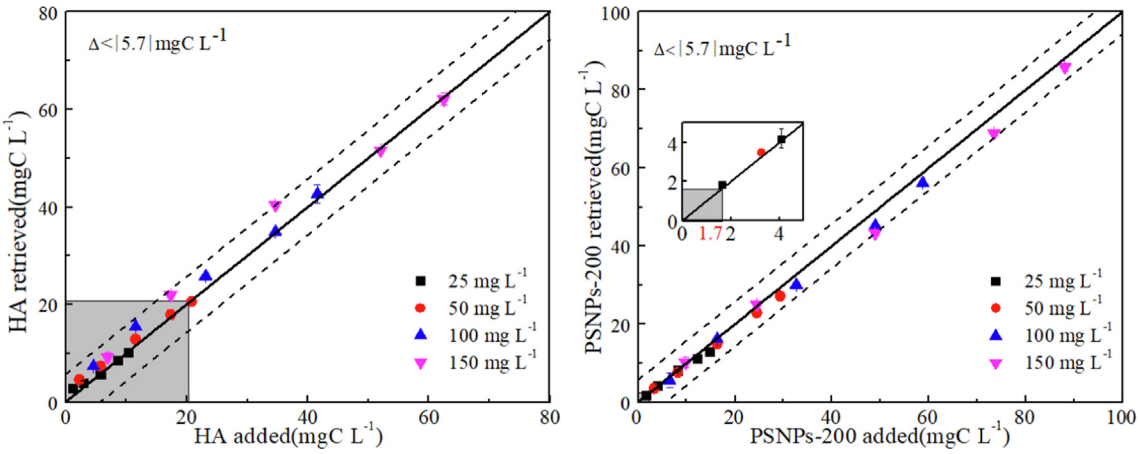

Fig. 2. Retrieved and nominal concentrations of HA and PSNPs-200 in their mixtures measured with the UV–Vis approach proposed using spectra covering the range of 231–600 nm. The solid line indicates the 1:1 line, and the dashed lines indicate boarders with an uncertainty (Δ) of ± 5.7 mgC L^{-1}. The grey shadowed area indicates that larger deviations (>16 %) can be found at lower concentrations (<20.8 mgC L^{-1} for HA and < 1.7 mgC L^{-1} for PSNPs-200).

with PSNPs–COOH-200 than with PSNP-200. A recovery of 100 ± 16 % could be achieved at an FA detection limit of 2.5 mgC L^{-1} and PSNPs–COOH-200 detection limit of 1.9 mgC L^{-1} (Fig. S8b), whereas in the FA and PSNPs-200 system the same recovery could be obtained with FA and PSNPs-200 detection limits of 7.5 and 4.1 mgC L^{-1}, respectively (Fig. S8a).

3.1.4. Effects of PSNPs size

PSNPs-400 exhibited a different UV–Vis spectrum than PSNPs-200, with a lower specific absorbance over the 200–280 nm wavelength range and a higher specific absorbance over 280–600 nm (Fig. S9). Specifically, the PSNPs-400 peak was lower and broader than that of PSNPs-200 and the top of the peak shifted from 228 to 252 nm.

Similar to the other treatments, better accuracy was obtained based on the spectra over the 231–600 nm wavelength range for the HA and PSNPs-400 mixtures (Table S5). Moreover, the derived concentrations of HA and PSNPs-400 were in agreement with the known added concentrations with absolute error < |3.7| mgC L^{-1} (Fig. S8d). The relative error was <16 % at an HA detection limit of 17.3 mgC L^{-1} and PSNPs-400 detection limit of 4.1 mgC L^{-1}. These limits of detection are somewhat lower than those in the mixtures with smaller PSNPs (PSNPs-200). The better accuracy for the larger PSNPs might be due to their smaller specific surface area, resulting in decreased interactions with NOM [25].

3.1.5. Ternary system of original HA, FA, and PSNPs

In the natural environment, HA and FA are often present simultaneously. Thus, the established UV–Vis method was further tested in a ternary system consisting of HA, FA, and PSNPs. Accordingly, another NOM composite was introduced into Eq. (2b) to calculate the concentrations of HA, FA, and PSNPs (Eq. S1 and S2). As expected, the more complicated ternary system required higher HA, FA, and PSNPs–COOH-200 detection limits (13.9, 8, and 7.4 mgC L^{-1}; Table S6 and Fig. S10) than the binary system (8.7, 2.5, and 3.7 mgC L^{-1}; Fig. S8c and S8b) to obtain the same recovery (100 ± 16 %), which might result from the complex interactions among the components (HA, FA, and NPs) and the similar spectra of HA and FA.

3.2. Mixtures of fractionated NOM with PSNPs

3.2.1. UV–Vis spectra of fractionated NOM

The DOC-normalized UV–Vis spectra of HA-F and FA-F are shown in Fig. 3a and 3c, respectively. Compared to that of HA and FA, the specific absorbance of HA-F and FA-F decreased while the shape of the spectra showed minimal change, similar to the findings of Xu et al. [49]. The first order derivatives of the DOC-normalized spectra revealed only slight differences between the original and fractionated HA and FA, further confirming that the spectra shape remained largely unaltered following adsorption to goethite (Fig. 3b and 3d). Therefore, the determination of the fractionated NOM and PSNPs could still be based on the shape of their spectra of the original NOM using Eq. (2b).

3.2.2. Binary system of HA-F and PSNPs

To obtain the same accuracy (100 ± 16 %), higher concentrations of HA and PSNPs were required for the HA-F compared to that of HA. For example, in the mixture of HA-F350 and PSNPs-200, detection limits of 34.7 and 49 mgC L^{-1} were required respectively to reach a relative error of < 16 % (Table S7 and Fig. S11a). Consistent with the HA and PSNPs systems, the UV–Vis method could be better applied with HA-F in the presence of PSNPs with carboxylic groups (PSNPs–COOH-200). A recovery of 100 ± 16 % for HA-F350 and PSNPs–COOH-200 could be achieved with detection limits of 23.1 and 7.4 mgC L^{-1}, respectively (Table S7 and Fig. S11b). The lower accuracy of the method for HA-F than that of HA could be attributed to several factors: 1) HA with higher charge density was preferentially adsorbed onto goethite [41], leaving the less charged and more hydrophobic HA (HA-F) in solution, which may interact with PSNPs to a greater degree than HA; 2) there are differences between the spectra of the original HA and HA-F (Fig. 3a), although $R_{NOM(i)}$ used in Eq. (2b) was acquired by the original HA. Additionally, the reliability of the method decreased for the mixture of HA-F250 and PSNPs-COOH-200 compared with that in the presence of HA-F350 (Table S7 and Fig. S11c). The higher degree of adsorption to goethite for HA-F250 (52.7 % adsorbed) than HA-F350 (33.3 % adsorbed; Table S1) likely led to larger changes in the properties and spectra of HA-F250, which then interfered with the measurement.

3.2.3. Binary system of FA-F and PSNPs

FA-F samples with different initial FA concentrations (FA-F250 and FA-F200) were selected to mix with PSNPs-COOH-200 to further test the UV–Vis method. The retrieved concentrations of FA-F250 and PSNPs-COOH-200 agreed with the known added concentrations for FA-F250 and PSNPs–COOH-200 detection limits of 16.0 and 5.9 mgC L^{-1}, respectively (Table S8 and Fig. S11d). However, for the FA-F200 and PSNPs–COOH-200 system, a deviation of < 16 % could only be achieved with FA-F200 and PSNPs–

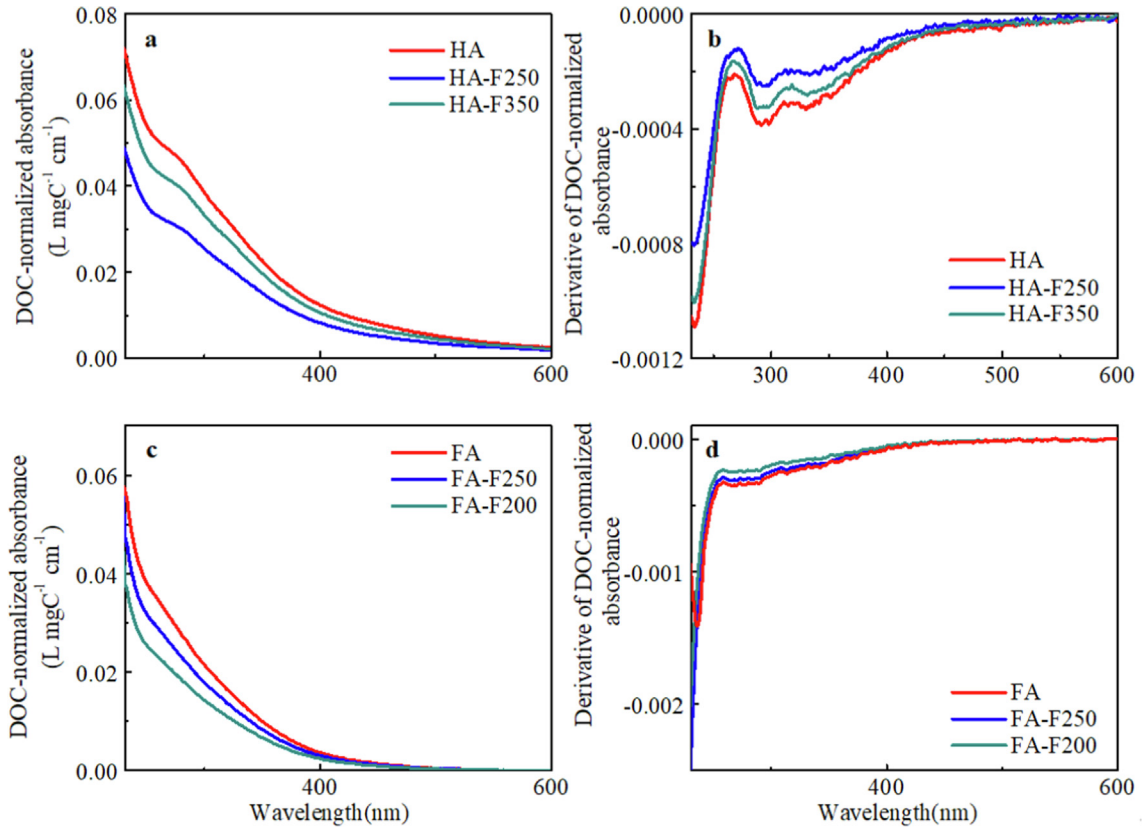

Fig. 3. Carbon normalized UV–Vis spectra and derivatives of the DOC-normalized UV–Vis spectra of the original HA (a) and fractionated HA (b) as well as original FA (c) and fractionated FA (d).

COOH-200 detection limits of 23.9 and 14.6 mgC L^{-1}, respectively (Table S8 and Fig. S11e), further indicating that the fractionation degree of NOM following interaction with the iron oxide influenced the accuracy of the UV–Vis method.

3.2.4. Ternary system of HA-F, FA-F, and PSNPs

The UV–Vis method was next applied to a ternary system containing HA-F350, FA-F250, and PSNPs-COOH-200 at a total concentration of 150 mg L^{-1} (see Section 2) and the data were processed according to Eq. S1 and S2. However, the relative error of this method was within 16 % for only HA-F350, FA-F250, and PSNPs-COOH-200 detection limits of 31.2, 18, and 27.5 mgC L^{-1}, respectively (Table S9 and Fig. S12), which were higher than those in the binary systems with PSNPs–COOH-200 and HA-F350 (23.1 mgC L^{-1} for HA-F350 and 7.4 mgC L^{-1} for PSNPs–COOH-200; Fig. S11b) or FA-F250 (16 mgC L^{-1} for FA-F250 and 5.9 mgC L^{-1} for PSNPs–COOH-200; Fig. S11d).

Thus, compared to the original NOM, fractionated NOM exhibited lower absorbance values and interacted more strongly with PSNPs owing to its higher hydrophobicity, leading to larger measurement errors. Additionally larger NOM fractionation degrees resulted in larger deviations of the calculated values from the known added values. Nevertheless, our results indicate that the UV–Vis method is an appropriate analytical methodology (within a 16 % error) for quantifying the concentrations of PSNPs and original and fractionated NOM in a mixture when their detection limits are high (20.8 mgC L^{-1} for NOM and 7.4 mgC L^{-1} for PSNPs in the NOM and PSNPs systems as well as 31.2 mgC L^{-1} for NOM and 27.5 mgC L^{-1} for PSNPs in fractionated NOM and PSNPs systems) and the fractionation degree of NOM is small (<33.2 %).

3.3. Proportion of NOM that interacts with PSNPs

The UV–Vis method developed here determines the total contents of NOM and PSNPs in the mixture while making no distinction between the "adsorbed" versus the "free" (not interacting with PSNPs) NOM. Thus, HA was added at a series of concentrations to equivalent amounts of PSNPs. In this experiment, PSNPs-400 were used as they could be filtered to determine the "free" NOM concentration using TOC analysis and the proportion of NOM that interacts with PSNPs could be further calculate (P_2 in Fig. 4 and Table S10), which was used to validate the results using the UV–Vis spectra (Section 2.3.3). Assuming that the special absorbance of HA adsorbed to PSNPs ($R_{\text{HA-ad(i)}}$) is negligible (see Eq. S3 and Fig. S13a), whereas those of HA in solution and PSNPs remain the same as the spectra of their original samples (Fig. S6a). The following equations (Eq. (3a) and (3b)), modified from Eq. (2b), were used to calculate the percentage of HA adsorbed to PSNPs (P_1%). P_1 was then compared with the results obtained using the filtration method (P_2).

$$A_{\text{MIX(i)}} = A' R_{\text{HA(i)}} + B' R_{\text{PSNPs(i)}} \tag{3a}$$

$$P_1 = \frac{V_{\text{HA}} + V_{\text{PSNPs}} - (A' + B')}{V_{\text{HA}}} \tag{3b}$$

where $A_{\text{MIX(i)}}$ (cm^{-1}) represents the absorbance of the mixture sample measured at a certain wavelength i nm, and $R_{\text{HA(i)}}$ (L mgC^{-1} cm^{-1}) and $R_{\text{PSNPs(i)}}$ (L mgC^{-1} cm^{-1}) are the specific absorbance of NOM or PSNPs in the reference spectra at a certain wavelength i nm. A' (mgC L^{-1}) and B' (mgC L^{-1}) can be obtained by fitting the equation to the spectra of the mixture of HA and PSNPs, minimizing the sum of squared differences between the measured and calculated total

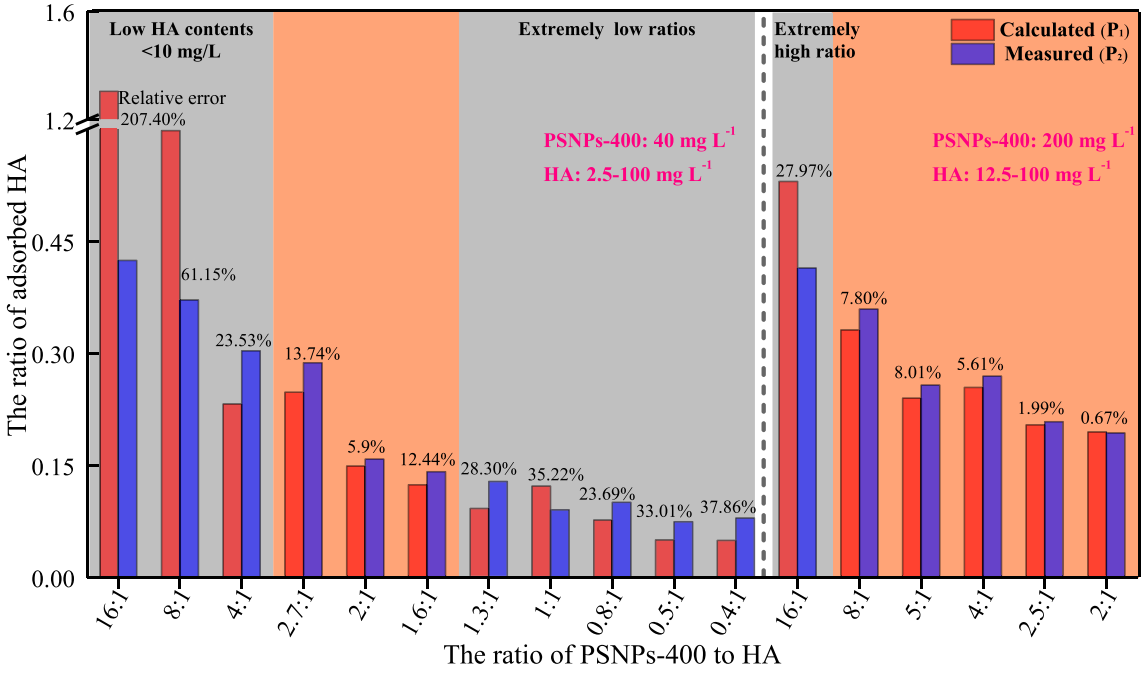

Fig. 4. Adsorption percentage derived from Eq. (3a) and (3b) using the UV–Vis spectra over 231–600 nm (P_1) and adsorption percentage obtained by TOC method (P_2) at different ratios of PSNPs-400 to HA. Smaller deviations (<13.7 %) can be found in the orange shadowed area, and the grey shadowed area indicates higher relative error (>13.7 %). (For interpretation of the references to colour in this figure legend, the reader is referred to the web version of this article.)

absorbance $\left(\Sigma\left(A_{MIX(i)} - A_{MIX(i)(model)}\right)^2\right)$ over the selected wavelength range. A' represents the concentration of "free" HA; B' represents the concentration of PSNPs. P_1 represents the percentage of HA that was adsorbed to PSNPs, and V_{HA} and V_{PSNPs} are the added concentrations of HA and PSNPs, resepectively. Based on the results discussed, the calculation was fitted using the spectra over 231–600 nm.

Under constant PSNPs-400 concentration (40 mg L^{-1}), the P_1 was in reasonable agreement with P_2 at an initial HA concentration of ≥ 10 mg L^{-1} (4.6 mgC L^{-1}; Fig. 4 and Table S10). In general, P_1 was lower than P_2, which could be explained by the assumption that the adsorbed HA does not contribute to the measured light absorbance. The relative error was lower (5.9–13.7 %) with higher mass ratios of initial PSNPs to HA (>1.6:1), whereas the error increased (23.7–37.9 %) with a decrease in the mass ratios of PSNPs to HA (≤1.3:1) despite the initial HA concentration being ≥ 30 mg L^{-1} (Fig. 4 and Table S10). HA adsorption onto PSNPs could be represented by the Freundlich isotherm; the high-energy sites of the PSNPs were occupied first, followed by lower-energy sites [43]. With a decrease in the mass ratios of PSNPs to HA, the loading of HA on PSNPs increased; accordingly, lower-energy sites might be occupied and could not quench the special light absorbance of adsorbed HA ($R_{HA-ad(i)}$) completely. Thus, a larger deviation between $R_{HA-ad(i)}$ and the assumed negligible light absorbance of adsorbed HA was observed (Fig. S13b), leading to bigger relative errors between the calculated and measured values. To further verify the assumption that the mass ratios of PSNPs to HA constituted a crucial factor for the performance of the UV–Vis method, the concentration of PSNPs-400 was further increased to 200 mg L^{-1}, then mixed with different concentrations of original HA (12.5, 25, 40, 50, 80, and 100 mg L^{-1}) to increase the mass ratios of PSNPs to HA. The relative errors (0.7–8.0 %) were acceptable with the higher mass ratios of PSNPs to HA (2:1–8:1; Fig. 4 and Table S10), consistent with the posited mechanism. However, the relative errors increased to 28.0 % when the mass ratio of PSNPs to HA increased to 16:1, possibly caused by the very low amount of HA left unadsorbed (Section 3.1.2). Therefore, the accuracy of the UV–Vis method can be affected by the mass ratios of PSNPs to HA and by HA concentration. Better estimation (relative errors < 13.7 %) of the HA proportion that reacted with NPs could be obtained with mass ratios of PSNPs to HA between 1.6:1 and 8:1 and HA concentrations of > 10 mg L^{-1} (4.6 mgC L^{-1}) under the experimental conditions evaluated (Fig. 4 and Table S10).

4. Conclusion

This study established a convenient and easily assessable method based on the UV–Vis spectrum and TOC analysis to quantify the concentrations of PSNPs and NOM (HA and FA) without and following adsorptive fractionation by an iron oxide (goethite, α-FeOOH); the proportion of HA interacting with the PSNPs was also estimated. The accuracy of the method depends on the type and fractionation degree of NOM, and on the functional groups and particle size of NPs. The relative error is within 16 % when the concentrations of NOM and NPs are higher than 20.8 mgC L^{-1} and 7.4 mgC L^{-1} respectively for the original NOM and PSNPs systems and higher than 31.2 mgC L^{-1} and 27.5 mgC L^{-1} respectively for fractionated NOM and PSNPs systems. Additionally, this UV–Vis method can better estimate the proportion of HA that reacted with NPs for NPs-to-HA mass ratios between 1.6:1 and 8:1 and HA concentrations of > 4.6 mgC L^{-1} under the experimental conditions evaluated. The methodology established here serves as a foundation to facilitate future laboratory-based research on the interactions among NOM, NPs, and iron oxides, although further studies are still needed to improve the performance of this method and to broaden the application of this method. In the future, fluorescent spectrometry can be combined with UV–Vis method to determine the concentration of NOM in the mixture. In addition, the content of N, S, and P elements in mixtures can be measured to increase the accurancy of NOM content determination.

CRediT authorship contribution statement

Ran Zhang: Investigation, Methodology, Writing – original draft. **Yali Chen:** Conceptualization, Writing – review & editing,

Funding acquisition. **Xiaoxue Ouyang:** Investigation. **Liping Weng:** Conceptualization, Methodology, Supervision, Writing – review & editing, Funding acquisition. **Jie Ma:** Resources. **Md. Shafiqul Islam:** Resources. **Yongtao Li:** Supervision, Resources.

Data availability

The data that has been used is confidential.

Declaration of Competing Interest

The authors declare that they have no known competing financial interests or personal relationships that could have appeared to influence the work reported in this paper.

Acknowledgements

The study is financially supported by the Central Public-interest Scientific Institution Basal Research Fund (2022-jbkyywf-cyl), the Key Projects at the Institute of Innovation Engineering, and the National Key Research and Development Program of China (2021YFD1700904).

Appendix A. Supplementary material

Supplementary data to this article can be found online at https://doi.org/10.1016/j.jcis.2022.11.050.

References

[1] J.R. Jambeck, R. Geyer, C. Wilcox, T.R. Siegler, M. Perryman, A. Andrady, R. Narayan, K.L. Law, Marine pollution. Plastic waste inputs from land into the ocean, Science 347 (6223) (2015) 768–771.
[2] A.L. Dawson, S. Kawaguchi, C.K. King, K.A. Townsend, R. King, W.M. Huston, S. M. Bengtson Nash, Turning microplastics into nanoplastics through digestive fragmentation by Antarctic krill, Nat. Commun. 9 (1) (2018) 1001.
[3] A.L. Andrady, Microplastics in the marine environment, Mar. Pollut. Bull. 62 (8) (2011) 1596–1605.
[4] D.K. Barnes, F. Galgani, R.C. Thompson, M. Barlaz, Accumulation and fragmentation of plastic debris in global environments, Philos. Trans. R. Soc. Lond. B Biol. Sci. 364 (1526) (2009) 1985–1998.
[5] M.C. Rillig, A. Lehmann, Microplastic in terrestrial ecosystems, Science 368 (6498) (2020) 1430–1431.
[6] J. Gigault, A.T. Halle, M. Baudrimont, P.Y. Pascal, F. Gauffre, T.L. Phi, H. El Hadri, B. Grassl, S. Reynaud, Current opinion: what is a nanoplastic?, Environ Pollut. 235 (2018) 1030–1034.
[7] J.M. Panko, J. Chu, M.L. Kreider, K.M. Unice, Measurement of airborne concentrations of tire and road wear particles in urban and rural areas of France, Japan, and the United States, Atmos. Environ. 72 (2013) 192–199.
[8] J.P. da Costa, P.S.M. Santos, A.C. Duarte, T. Rocha-Santos, (Nano)plastics in the environment - sources, fates and effects, Sci. Total Environ. 566–567 (2016) 15–26.
[9] L. Nizzetto, G. Bussi, M.N. Futter, D. Butterfield, P.G. Whitehead, A theoretical assessment of microplastic transport in river catchments and their retention by soils and river sediments, Environ. Sci.-Proc. Imp. 18 (8) (2016) 1050–1059.
[10] V. Hidalgo-Ruz, L. Gutow, R.C. Thompson, M. Thiel, Microplastics in the marine environment: a review of the methods used for identification and quantification, Environ. Sci. Technol. 46 (6) (2012) 3060–3075.
[11] R. Dris, J. Gasperi, V. Rocher, M. Saad, N. Renault, B. Tassin, Microplastic contamination in an urban area: a case study in Greater Paris, Environ. Chem. 12 (5) (2015) 592–599.
[12] L. Nizzetto, M. Futter, S. Langaas, Are agricultural soils dumps for microplastics of urban origin?, Environ Sci. Technol. 50 (20) (2016) 10777–10779.
[13] A.G.J. Driedger, H.H. Durr, K. Mitchell, P. Van Cappellen, Plastic debris in the Laurentian Great Lakes: a review, J. Great Lakes Res. 41 (1) (2015) 9–19.
[14] C.M. Rochman, C. Manzano, B.T. Hentschel, S.L. Simonich, E. Hoh, Polystyrene plastic: a source and sink for polycyclic aromatic hydrocarbons in the marine environment, Environ. Sci. Technol. 47 (24) (2013) 13976–13984.
[15] E.L. Teuten, J.M. Saquing, D.R. Knappe, M.A. Barlaz, S. Jonsson, A. Bjorn, S.J. Rowland, R.C. Thompson, T.S. Galloway, R. Yamashita, D. Ochi, Y. Watanuki, C. Moore, P.H. Viet, T.S. Tana, M. Prudente, R. Boonyatumanond, M.P. Zakaria, K. Akkhavong, Y. Ogata, H. Hirai, S. Iwasa, K. Mizukawa, Y. Hagino, A. Imamura, M. Saha, H. Takada, Transport and release of chemicals from plastics to the environment and to wildlife, Philos. Trans. R. Soc. Lond. B Biol. Sci. 364 (1526) (2009) 2027–2045.
[16] F.F. Liu, G.Z. Liu, Z.L. Zhu, S.C. Wang, F.F. Zhao, Interactions between microplastics and phthalate esters as affected by microplastics characteristics and solution chemistry, Chemosphere 214 (2018) 688–694.
[17] J. Wang, S. Coffin, C. Sun, D. Schlenk, J. Gan, Negligible effects of microplastics on animal fitness and HOC bioaccumulation in earthworm Eisenia fetida in soil, Environ. Pollut. 249 (2019) 776–784.
[18] L.A. Holmes, A. Turner, R.C. Thompson, Interactions between trace metals and plastic production pellets under estuarine conditions, Mar. Chem. 167 (2014) 25–32.
[19] M. Davranche, C. Veclin, A.-C. Pierson-Wickmann, H. El Hadri, B. Grassl, L. Rowenczyk, A. Dia, A. Ter Halle, F. Blancho, S. Reynaud, J. Gigault, Are nanoplastics able to bind significant amount of metals? The lead example, Environ. Pollut. 249 (2019) 940–948.
[20] C.M. Rochman, T. Kurobe, I. Flores, S.J. Teh, Early warning signs of endocrine disruption in adult fish from the ingestion of polyethylene with and without sorbed chemical pollutants from the marine environment, Sci. Total Environ. 493 (2014) 656–661.
[21] C.M. Rochman, E. Hoh, T. Kurobe, S.J. Teh, Ingested plastic transfers hazardous chemicals to fish and induces hepatic stress, Sci. Rep. 3 (1) (2013) 3263.
[22] L.G.A. Barboza, A. Dick Vethaak, B. Lavorante, A.K. Lundebye, L. Guilhermino, Marine microplastic debris: An emerging issue for food security, food safety and human health, Mar. Pollut. Bull. 133 (2018) 336–348.
[23] D.G. Lumsdon, A.R. Fraser, Infrared spectroscopic evidence supporting heterogeneous site binding models for humic substances, Environ. Sci. Technol. 39 (17) (2005) 6624–6631.
[24] C.S. Chen, C. Le, M.H. Chiu, W.C. Chin, The impact of nanoplastics on marine dissolved organic matter assembly, Sci. Total Environ. 634 (2018) 316–320.
[25] W. Chen, Z.Y. Ouyang, C. Qian, H.Q. Yu, Induced structural changes of humic acid by exposure of polystyrene microplastics: A spectroscopic insight, Environ. Pollut. 233 (2018) 1–7.
[26] R.F. Shiu, C.I. Vazquez, Y.Y. Tsai, G.V. Torres, C.S. Chen, P.H. Santschi, A. Quigg, W.C. Chin, Nano-plastics induce aquatic particulate organic matter (microgels) formation, Sci. Total Environ. 706 (2020).
[27] S. Dong, W. Cai, J. Xia, L. Sheng, W. Wang, H. Liu, Aggregation kinetics of fragmental PET nanoplastics in aqueous environment: Complex roles of electrolytes, pH and humic acid, Environ. Pollut. 268 (2021).
[28] T. Hiemstra, S. Mia, P.B. Duhaut, B. Molleman, Natural and pyrogenic humic acids at goethite and natural oxide surfaces interacting with phosphate, Environ. Sci. Technol. 47 (16) (2013) 9182–9189.
[29] M. Li, L. He, M.Y. Zhang, X.W. Liu, M.P. Tong, H. Kim, Cotransport and deposition of iron oxides with different-sized plastic particles in saturated quartz sand, Environ. Sci. Technol. 53 (7) (2019) 3547–3557.
[30] Y.Y. Zhang, Y.Y. Luo, X.T. Guo, T.J. Xia, T.C. Wang, H.Z. Jia, L.Y. Zhu, Charge mediated interaction of polystyrene nanoplastic (PSNP) with minerals in aqueous phase, Water Res. 178 (2020).
[31] L. Weng, W.H. van Riemsdijk, L.K. Koopal, T. Hiemstra, Adsorption of humic substances on goethite: comparison between humic acids and fulvic acids, Environ. Sci. Technol. 40 (24) (2006) 7494–7500.
[32] L. Weng, W.H. Van Riemsdijk, T. Hiemstra, Adsorption of humic acids onto goethite: effects of molar mass, pH and ionic strength, J. Colloid Interface Sci. 314 (1) (2007) 107–118.
[33] S. Kang, B.S. Xing, Humic acid fractionation upon sequential adsorption onto goethite, Langmuir 24 (6) (2008) 2525–2531.
[34] D.C. Olk, P.R. Bloom, E.M. Perdue, D.M. McKnight, Y. Chen, A. Farenhorst, N. Senesi, Y.P. Chin, P. Schmitt-Kopplin, N. Hertkorn, M. Harir, Environmental and agricultural relevance of humic fractions extracted by alkali from soils and natural waters, J. Environ. Qual. 48 (2) (2019) 217–232.
[35] N. Janot, P.E. Reiller, X. Zheng, J.P. Croue, M.F. Benedetti, Characterization of humic acid reactivity modifications due to adsorption onto alpha-Al_2O_3, Water Res. 46 (3) (2012) 731–740.
[36] L. Weng, W.H. Van Riemsdijk, L.K. Koopal, T. Hiemstra, Ligand and Charge Distribution (LCD) model for the description of fulvic acid adsorption to goethite, J. Colloid Interface Sci. 302 (2) (2006) 442–457.
[37] B. Gu, J. Schmitt, Z. Chen, L. Liang, J.F. McCarthy, Adsorption and desorption of natural organic matter on iron oxide: mechanisms and models, Environ. Sci. Technol. 28 (1) (1994) 38–46.
[38] A.W.P. Vermeer, W.H. van Riemsdijk, L.K. Koopal, Adsorption of humic acid to mineral particles. 1. Specific and electrostatic interactions, Langmuir 14 (10) (1998) 2810–2819.
[39] H.C. Xu, L. Ji, M. Kong, H.L. Jiang, J. Chen, Molecular weight-dependent adsorption fractionation of natural organic matter on ferrihydrite colloids in aquatic environment, Chem. Eng. J. 363 (2019) 356–364.
[40] X.P. Qin, F. Liu, G.C. Wang, H. Hou, F.S. Li, L.P. Weng, Fractionation of humic acid upon adsorption to goethite: Batch and column studies, Chem. Eng. J. 269 (2015) 272–278.
[41] L. Wang, Y.T. Li, L.P. Weng, Y. Sun, J. Ma, Y.L. Chen, Using chromatographic and spectroscopic parameters to characterize preference and kinetics in the adsorption of humic and fulvic acid to goethite, Sci. Total Environ. 666 (2019) 766–777.
[42] P. Reiller, B. Amekraz, C. Moulin, Sorption of Aldrich humic acid onto hematite: insights into fractionation phenomena by electrospray ionization with quadrupole time-of-flight mass spectrometry, Environ. Sci. Technol. 40 (7) (2006) 2235–2241.
[43] A. Abdurahman, K. Cui, J. Wu, S. Li, R. Gao, J. Dai, W. Liang, F. Zeng, Adsorption of dissolved organic matter (DOM) on polystyrene microplastics in aquatic

environments: Kinetic, isotherm and site energy distribution analysis, Ecotoxicol. Environ. Saf. 198 (2020).
[44] Z.F. Song, X.Y. Yang, F.M. Chen, F.Y. Zhao, Y. Zhao, L.L. Ruan, Y.G. Wang, Y.S. Yang, Fate and transport of nanoplastics in complex natural aquifer media: Effect of particle size and surface functionalization, Sci. Total Environ. 669 (2019) 120–128.
[45] M.M. Tan, L.F. Liu, M.G. Zhang, Y.L. Liu, C.Y. Li, Effects of solution chemistry and humic acid on the transport of polystyrene microplastics in manganese oxides coated sand, J. Hazard. Mater. 413 (2021).
[46] F. Zhang, Z. Wang, S. Wang, H. Fang, D.G. Wang, Aquatic behavior and toxicity of polystyrene nanoplastic particles with different functional groups: Complex roles of pH, dissolved organic carbon and divalent cations, Chemosphere 228 (2019) 195–203.
[47] K. Kaiser, G. Guggenberger, Sorptive stabilization of organic matter by microporous goethite: sorption into small pores vs. surface complexation, Eur. J. Soil Sci. 58 (1) (2007) 45–59.
[48] J. Peuravuori, K. Pihlaja, Molecular size distribution and spectroscopic properties of aquatic humic substances, Anal. Chim. Acta 337 (2) (1997) 133–149.
[49] Y. Xu, Y.l.N. Bai, T. Hiemstra, W.F. Tan, L.P. Weng, Resolving humic and fulvic acids in binary systems influenced by adsorptive fractionation to Fe-(hydr) oxide with focus on UV–Vis analysis, Chem. Eng. J. 389 (2020).
[50] A.M. Yasir, J. Ma, X. Ouyang, J. Zhao, Y. Zhao, L. Weng, M.S. Islam, Y. Chen, Y. Li, Effects of selected functional groups on nanoplastics transport in saturated media under diethylhexyl phthalate co-contamination conditions, Chemosphere 286 (2022).
[51] J.D. Filius, D.G. Lumsdon, J.C.L. Meeussen, T. Hiemstra, W.H. Van Riemsdijk, Adsorption of fulvic acid on goethite, Geochim. Cosmochim. Acta 64 (1) (2000) 51–60.
[52] L. Li, W. Huang, P.a. Peng, G. Sheng, J. Fu, Chemical and molecular heterogeneity of humic acids repetitively extracted from a peat, Soil Sci. Soc. Am. J. 67 (3) (2003) 740–746.
[53] T. Hiemstra, W.H. Van Riemsdijk, Surface structural ion adsorption modeling of competitive binding of oxyanions by metal (hydr)oxides, J. Colloid Interface Sci. 210 (1) (1999) 182–193.
[54] Y.L. Chen, J. Ma, Y.T. Li, L.P. Weng, Enhanced cadmium immobilization in saturated media by gradual stabilization of goethite in the presence of humic acid with increasing pH, Sci. Total Environ. 648 (2019) 358–366.
[55] J. Wu, R. Jiang, W. Lin, G. Ouyang, Effect of salinity and humic acid on the aggregation and toxicity of polystyrene nanoplastics with different functional groups and charges, Environ. Pollut. 245 (2019) 836–843.
[56] J. Hur, M.A. Williams, M.A. Schlautman, Evaluating spectroscopic and chromatographic techniques to resolve dissolved organic matter via end member mixing analysis, Chemosphere 63 (3) (2006) 387–402.